Biochimica et Biophysica Acta 1838 (2014) 890–901

Contents lists available at ScienceDirect

Biochimica et Biophysica Acta

journal homepage: www.elsevier.com/locate/bbamem

Interaction of a calix[4]arene derivative with a DOPC bilayer: Biomolecular simulations towards chloride transport

Paulo J. Costa [1], Igor Marques, Vítor Félix *

Departamento de Química, CICECO and Secção Autónoma de Ciências da Saúde, Universidade de Aveiro, Aveiro 3810-193, Portugal

ARTICLE INFO

Article history:
Received 1 March 2013
Received in revised form 25 November 2013
Accepted 26 November 2013
Available online 6 December 2013

Keywords:
Molecular dynamics simulation
Transmembrane chloride transport
Carrier mechanism
Calixarene
DOPC

ABSTRACT

The ability of a calix[4]arene derivative (**CX-1**), bearing four protonated $-NH_3^+$ groups located in the upper rim and aliphatic tails in the lower rim, to interact with a 1,2-dioleoyl-*sn*-glycero-3-phosphocholine (DOPC) model bilayer and promote transmembrane chloride transport was investigated by molecular dynamics (MD) simulations. Unconstrained MD simulations show that the interaction of **CX-1** with DOPC occurs *via* the $-NH_3^+$ groups, which are able to establish electrostatic interactions and multiple hydrogen bonds with the DOPC phosphate groups, while the aliphatic tails point towards the water phase (when **CX-1** starts from the water phase) or to the membrane (when **CX-1** is initially positioned within the bilayer). The interaction does not induce any relevant perturbation on the biophysical properties of the bilayer system (area per lipid, thickness, and hydration) apart from a systematic increase in the order parameter of the C2 carbon atom of the *sn-1* lipid tail, meaning that the bilayer conserves its integrity. Since total internalization of **CX-1** was not observed in the unconstrained MD time-scale, constant velocity steered molecular dynamics (SMD) simulations were performed in order to simulate the **CX-1** permeation across the bilayer. At pulling velocities lower than 0.0075 nm ps^{-1}, chloride transport was observed. The Potential of Mean Force (PMF), calculated with the weighted histogram analysis method, indicates a barrier of *ca.* 58 kJ mol^{-1} for this mobile carrier to cross the membrane.

© 2013 Elsevier B.V. All rights reserved.

1. Introduction

Several chemical entities, *e.g.* cholesterol [1], anesthetics [2] or ions [3], interact with the phospholipids of cell membranes, playing important roles in the metabolism. Concerning the latter species, regulation of cellular ion concentration is critical for human health and, for instance, misregulation of chloride cellular transport has been associated with several diseases such as myotonia, nephrolithiasis (kidney stones), Bartter's syndrome and cystic fibrosis [4]. Therefore, the development of synthetic molecules that act as small mobile carriers or static channels assisting transmembrane anion transport (in particular chloride) is of extreme importance due to their potential use in the treatment of these channelopathies, as illustrated by several comprehensive reviews on the subject [5,6].

Calixarene scaffolds (see **CX** in Scheme 1) are particularly interesting platforms, given their recognized ability to promote transmembrane ion transport as ion channels or mobile carriers [7]. Noticeably, a few decades ago, *p*-sulfonato-calix[*n*]arenes were reported to induce blockage of the colonic chloride channel, which increases with the size of the calixarene scaffold, as *n* assumes the values of 4, 6 or 8 [8]. This finding was subsequently used for the development of chloride channel modulators such as blockers of the outwardly rectifying chloride channel (ORCC) [9], showing that these *p*-sulfonato derivatives can act as channel-blocking drugs relevant for cystic fibrosis [10] and neurophysiology [11] research. Their biological application was also subjected to a review [12]. On the other hand, calix[4]arene compounds are known to form artificial anion channels. For instance, a derivative containing four cationic spermidine units on the upper rim and four non-polar benzyloxymethyl group appendages [13], as well as a calix[4]arene tetrabutylamide derivative [14], shows H^+/Cl^- symport activity. In both cases, the calix[4]arene skeleton adopts a 1,3-*alternate* conformation and the anion transport occurs through static ion channels formed by the calix[4]arene molecule spanning the entire membrane (first case) or by the assembly of two calix[4]arene units through two water bridges (second case). In contrast, the same calix[4]arene tetrabutylamide derivative, when exhibiting a cone conformation, is also able to transport chloride anions across phospholipid membranes, but as a mobile carrier [15].

The amphiphilic properties of calix[4]arenes make them relevant in biomedical applications as illustrated by the use of a fluorescent calix[4]arene derivative (**CX-F** in Scheme 1) for cell imaging. In fact, both **CX-F** and a control molecule **CX-1** (an anilinium calix[4]arene bearing four propoxy tails on the narrower rim, also sketched in Scheme 1), undergo cellular uptake, the specific mechanism being unclear, although caveolae-linked endocytosis or lipid-raft processes were experimentally excluded [16].

* Corresponding author at: Departamento de Química, Universidade de Aveiro, Aveiro 3810-193, Portugal. Tel.: +351 234370729.
E-mail address: vitor.felix@ua.pt (V. Félix).
[1] Current address: Departamento de Química, QOPNA and Secção Autónoma de Ciências da Saúde, Universidade de Aveiro, Aveiro 3810-193, Portugal.

0005-2736/$ – see front matter © 2013 Elsevier B.V. All rights reserved.
http://dx.doi.org/10.1016/j.bbamem.2013.11.021

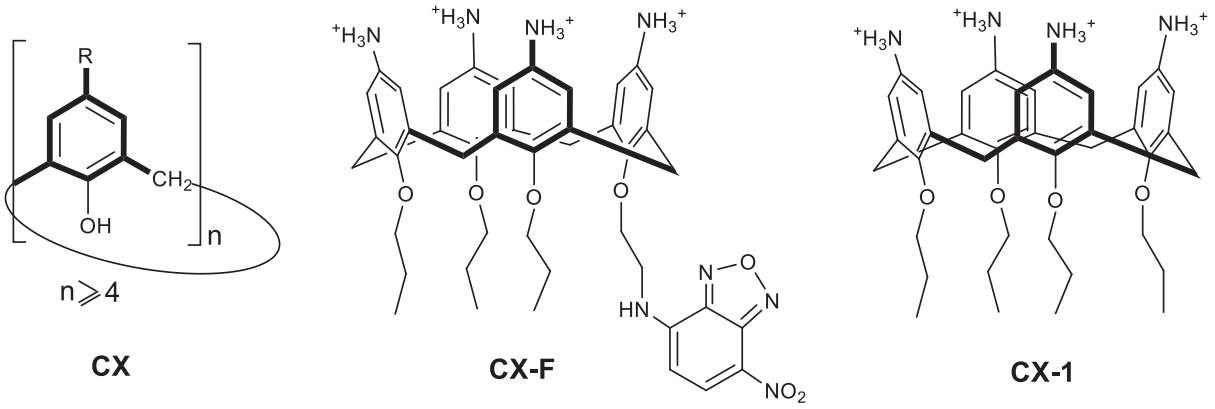

Scheme 1. Structures of the general calixarene scaffold **CX** and calix[4]arene derivatives **CX-F** and **CX-1**.

This amphiphilic calixarene design with polar headgroups at the upper rim and nonpolar tails in the lower rim, besides allowing self-assembling in monolayers [17], was also shown to enable insertion in lipid monolayers for biochemical applications as reported by Schrader and co-workers [18]. In particular, for the anionic tetraphosphonate calix[4]arene with four tetrabutoxy tails on the lower rim, the experiments clearly show an obvious and preferential parallel orientation of the calixarene amphiphilic molecule inside the monolayer. More importantly, the four negative tetraphosphonate groups are able to recognize proteins *via* a multiple cooperative recognition phenomenon [19]. This idea was extended to cationic benzylammonium or anilinium calix[4]arenes with four tetrabutoxy tails, which were embedded into a stearic acid monolayer [20]. The latter compound is very similar to **CX-1**, having one less carbon atom on each tail. The ammonium groups form salt bridges and ion-pairs reinforced by hydrogen bonds with aspartates and glutamates in protein recognition. This concept enables inclusively the "naked eye" color detection of proteins [21].

Similarly to what happens in protein recognition, in **CX-1** the four protonated $-NH_3^+$ groups located in the upper rim can potentially act as anion binders through the formation of ion-pairs with phosphate headgroups complemented by P = O···N – H hydrogen bonding interactions, while the aliphatic tails in the lower rim provide the lipophilic part enabling the membrane internalization. Therefore, **CX-1** can be seen as a prototype of an anion transporter by the mobile carrier mechanism, much like the calix[4]arene reported in reference [15]. Unfortunately, to the best of our knowledge, the anion transport ability of both **CX-F** and **CX-1** was not yet experimentally measured.

Consequently, and given our interest in both calixarene chemistry [22] and transmembrane anion transport [23,24], in this paper we sought to explore the possible role of **CX-1** in chloride transmembrane transport using Molecular Dynamics (MD) simulations. This type of simulations has become an increasingly powerful tool for the investigation of the interaction of several molecules with phospholipid bilayers, ranging from anesthetics and nonimmobilizers [25,26], β-blockers [27], amino acids such as arginine [28] or peptides [29,30], to polycyclic aromatic hydrocarbons like pyrene [31]. But regarding the anion transport mediated by synthetic anion transporters, MD simulations are scarce with only a few studies, mainly reported by our group [23,24]. These simulation studies might be hindered by the fact that those transporters possess a wide variety of chemical groups, thus making the development of specific force field (FF) parameterization for the transporter consistent with the force field used for phospholipid bilayer an eventual issue. Therefore, besides exploring the role of **CX-1** in chloride transmembrane transport, this paper also aims to confirm the applicability of the General Amber Force Field (GAFF) [32] in biomoloecular simulations of phospholipid membranes interacting with a given organic molecule.

2. Simulation details

2.1. Theoretical background

For the biomolecular simulation of phospholipid bilayers there are several FFs currently available, such as the recently updated all-atom Chemistry at HARvard Molecular Mechanics (CHARMM) parameter set, named CHARMM36 [33] or the GROningen MOlecular Simulation (GROMOS) united-atom G53A6 version [34,35], labeled $G53A6_L$. Among the FFs of the AMBER family, the General Amber Force Field (GAFF) [32] has the advantage of being virtually applicable to any organic molecule, however it was not used in phospholipid simulations until 2007, when Martinek and co-workers [36] reported a study on a 1-palmitoyl-2-oleoyl-*sn*-glycero-3-phosphocholine (POPC) bilayer system composed of 128 lipids and 2985 TIP3P [37] water molecules, showing that the experimental properties were properly reproduced when an NPγT ensemble is used ($\gamma = 60$ mN m^{-1} per bilayer, 30 dyn cm^{-1} per surface). After this seminal paper, other groups have extended the GAFF application, namely, Gould and co-workers [38] which performed a systematic test on fully hydrated 1,2-dimyristoyl-*sn*-glycero-3-phosphocholine (DMPC) and 1,2-dioleoyl-*sn*-glycero-3-phosphocholine (DOPC) bilayers composed of 72 lipids and 2449 or 2935 TIP3P water molecules, respectively. It was shown that GAFF reproduces several representative liquid phase properties of the structure and dynamics of DMPC and DOPC in an NPT ensemble, however, the calculated areas per lipid were systematically underestimated when compared with the experimental values. Almost simultaneously, Böckmann and co-workers [39] used GAFF together with the Berendsen weak-coupling algorithm in simulations of a DOPC bilayer composed of 72 lipids and 2727 TIP3P or SCP/E [40] water molecules. GAFF was the only FF, among those studied, that displayed the experimentally observed difference in the order of the C2 atom between the two acyl chains. Moreover, in an NPγT ensemble ($\gamma = 22$ dyn cm^{-1} per surface), the calculated DOPC area per lipid perfectly matches the experimental value of 0.72 nm^2, especially when the SPC/E water model is used. Notice that the weak-coupling algorithm used in this study does not yield a correct NPγT statistical ensemble; nevertheless, we decided to keep the NPγT nomenclature, which is commonly adopted when the membrane simulations are performed with this algorithm as illustrated by the reference [39]. In this work, the authors also highlighted the fact that those developments allow the systematic study of the partition of arbitrary solutes between the solvent and the bilayer. Indeed, the parameterization of arbitrary organic molecules such as the ones present in drug libraries or the above mentioned synthetic anion transporters, is feasible but not straightforward in the framework of $G53A6_L$, although tools like the Automated Topology Builder (ATB) [41] are available. For CHARMM, there is a newly developed CHARMM General Force Field (CGenFF)

[42] with an online server [43], which puts a stronger emphasis on quantum mechanical (QM) calculations in the parameterization philosophy including the atomic charge calculation in the presence of a given number of water molecules. This surely increases accuracy but could also increase the time spent parameterizing an arbitrary organic molecule. In contrast, the GAFF, in conjunction with the freely available Antechamber module of AmberTools [44], allows the user to generate an Amber compatible topology very easily and quickly which could be important for drug screening methods. In light of these developments, in this study, GAFF parameters were used for both lipids and **CX-1** as explained below.

2.2. Bilayer setup and parameters

From the reported phospholipid bilayer MD simulations with GAFF, we have chosen the DOPC + SPC/E combination which gave very good results for several biophysical lipid parameters [39].

The initial system was composed of an all-atom DOPC membrane with 72 lipids and 2727 SPC/E water molecules, taken from Ref. [39]. In order to include **CX-1** in the water phase, this previously equilibrated membrane model was expanded along the *z* axis direction (bilayer normal) by the addition of an equal number of water molecules to both water slabs with Packmol [45], leading to an overhydrated membrane system with a total of 6117 water molecules. Henceforth, this membrane model is denoted as system **A**. The DOPC parameters (GAFF) and atomic charges, in the form of GROMACS topologies were also taken from Ref. [39].

2.3. **CX-1** *parameters*

The **CX-1** is conformationally locked in a *cone* conformation and therefore, a *cone* **CX-1** molecular model was built and geometry optimized at the B3LYP/6-31G* level of theory using Gaussian09 [46]. RESP atomic charges were then fitted to the electrostatic potential obtained at the HF/6-31G* using 4 concentric layer of points per atom and 6 points per unit area (Gaussian IOP 6/33 = 2, 6/41 = 4, 6/42 = 6) in agreement with the methodology proposed in the force field reference [32] by post-processing the G09 output with the Antechamber module of AmberTools [44]. The resulting charges are presented in Fig. S1 in Supplementary Data together with the GAFF atom types, which were automatically assigned with AmberTools. Subsequently, eventual atom type inconsistencies were *manually* checked. The resulting AMBER topology files were converted into GROMACS topologies using the *acpype.py* tool [47].

2.4. Simulation conditions and data analysis

All MD simulations were performed with GROMACS 4.5.3 package [48] adapting the protocol presented in Ref. [39] as follows. All systems were simulated in rectangular boxes under periodic boundary conditions at 310 K using the Berendsen thermostat [49] by separately coupling the lipids and the water molecules to a bath with time constant of 0.1 ps^{-1}. The long-range electrostatic interactions were treated with the Particle Mesh Ewald (PME) algorithm [50] with a 1.0 nm cut-off. The cut-off for the Lennard–Jones interactions was also set at 1.0 nm, while the non-bonded pair list was updated every 10 steps. The pressure was maintained constant at 1 atm, controlled by the Berendsen barostat with a coupling constant of 1.0 ps. Independent coupling in the *x*, *y* and *z* directions was used and a surface tension γ of 22 dyn cm^{-1} per surface was applied. The volume compressibility was set to 4.5×10^{-5} bar^{-1}. All covalent bonds to hydrogen atoms were constrained using the LINCS [51] algorithm for DOPC and **CX-1** and the SETTLE [52] algorithm for water molecules, allowing the use of a 2 fs time-step.

The system **A** was energy minimized in a two-step procedure using the steepest descent method until machine precision was reached. In the first step the lipid molecules were restrained (1000 kJ mol^{-1} nm^{-2}) in order to accommodate the added water molecules. The second step consisted in the minimization of all the system to remove eventual bad contacts. The system was then simulated for 100 ns in an NPγT ensemble with initial velocities generated according to a Maxwell distribution at 310 K. Only one replicate was performed since the results obtained were virtually identical to the previously ones reported in Ref. [39], apart of small differences arising from the system size, derived from the different number of water molecules (see below). This simulation was further used as reference to evaluate the impact of **CX-1** on the structural and dynamic properties of the DOPC membrane model.

The system **A** was used as template for the subsequent MD simulations as follows. **CX-1** was randomly placed in the water slab at a distance larger than 1.0 nm from the closest water/lipid interface leading to system **B**. This intends to reduce any *bias* that any chosen **CX-1** initial orientation might induce on the **CX-1**/lipid interactions. Therefore, in the beginning of the simulation, the phospholipids are not able to "see" **CX-1**, which diffuses in the water phase free of any direct intermolecular interactions with the phospholipid heads. The system **B** was also minimized in two stages as **A**, except that in the first 5 ns of the MD simulation, a weak positional restraint (1000 kJ mol^{-1} nm^{-2}) was applied to **CX-1**. Afterwards, the restraint was released and the simulation continued for 100 ns. In order to increase the sampling, two additional replicates of 100 ns were performed for system **B** using different random seeds for the initial velocities, thus leading to a total simulation time of 300 ns.

An additional system **C** was built by the carefully insertion of **CX-1** in the middle of the membrane, gently moving some of the lipid tails in order to accommodate the calix[4]arene. The system was also further energy minimized in two steps. In the first step, the lipids were allowed to relax while the structure **CX-1** was restrained through a positional restraint of 1000 kJ mol^{-1} nm^{-2}. This procedure enables the lipid tails to accommodate **CX-1** with a substantial reduction of the bad contacts. The second stage consisted on the minimization of the entire system. Then, a short 5 ns simulation was performed keeping **CX-1** positioned in the middle of the phospholipid bilayer with a positional restraint of 1000 kJ mol^{-1} nm^{-2}. This simulation allowed the lipids to definitively adapt to the **CX-1** presence before the data collection. Finally a 100 ns simulation without any restraints was performed. As in system **B**, two additional replicates of 100 ns were also performed.

The electro-neutrality of systems **B** and **C** was achieved by the addition of four chloride anions (charge −1) with van der Waals parameters taken from Ref. [3]. These anions were randomly positioned in the water phase. Overall, excluding the short 5 ns relaxation, a total of 700 ns of MD simulation time was performed for the systems **A**, **B** and **C** as summarized in Table S1. Unless explicitly stated, the first 20 ns of each unconstrained MD run were considered equilibration time and were discarded from the subsequent phase production. The results were analyzed using the GROMACS 4.5.3 built-in tools or with in-house custom scripts, unless otherwise stated.

2.5. Pulling simulations

The events that occur during the **CX-1** permeation across the membrane were mimicked by the use of constant velocity steered molecular dynamics (SMD) simulations. An equilibrated snapshot of each replicate of **B** was taken and the center of mass (COM) of **CX-1** was pulled in the *z* direction (normal to the bilayer plane), forcing the calix[4]arene to move from the water phase and permeate the DOPC bilayer towards the middle of the membrane. A harmonic potential with a force constant of 1000 kJ mol^{-1} nm^{-2} was used along with constant velocities of 0.01, 0.0075, 0.005, and 0.001 nm ps^{-1}.

2.6. Umbrella sampling

The Umbrella Sampling procedure [53] combined with the weighted histogram analysis method (WHAM) [54] was used to compute the Potential of Mean force (PMF) profile for the **CX-1** translocation across the DOPC bilayer. Initially, an equilibrated snapshot from system **B** was taken and used to pull **CX-1** from water to the center of the membrane core, building the individual simulation windows. However, this approach led to irreversible pulling of some phospholipid heads which interfere with the PMF profile (see Supporting Information). In order to avoid this, the reverse process was undertaken using an equilibrated snapshot from system **C** and pulling the receptor from the membrane center to the water phase in order to build the simulation windows. A similar strategy was employed to study the PMF profile of the transportan peptide across a DPPC bilayer [55].

A harmonic restraint with force constant of 3200 kJ mol^{-1} nm^{-2} was applied to the distance, in the z direction, between the COM of **CX-1** and the COM of the DOPC bilayer. 30 windows equally separated by 0.15 nm were generated and each window was independently simulated during 10 ns. The first 2 ns were discarded as equilibration period. After the simulations were completed, the unbiased Potential of Mean Force (PMF) was obtained using the WHAM method implemented in *g_wham*. In this analysis tool, the statistical errors are calculated by the bootstrap analysis technique [56]. Succinctly, bootstrapping estimates the unknown probability distribution $P(a)$ using a set of n observations for a quantity $A(a_1, \ldots, a_n)$. This is subsequently used to generate new random sets of n hypothetical observations based on that estimated distribution. The uncertainty is estimated based on the standard deviation of the hypothetical values of A. Thus, for a PMF as reported herein, bootstrapped trajectories $\zeta_{b,i}(t)$ are generated according to the umbrella histograms of the simulations trajectories $\zeta_i(t)$. The bootstrapped trajectories are further used to generate their own histograms and bootstrapped PMF $W_b(\zeta)$, the process being repeated N_b times to generate $W_{b,k}(\zeta)$ PMFs (with $k = 1, \ldots, N_b$). Finally, the uncertainty $\sigma_{PMF}(\zeta)$ is given by

$$\sigma_{PMF}(\zeta) = \left[(N_b - 1)^{-1} \sum_{k=1}^{Nb} \left(W_{b,k}(\zeta) - \langle W_b(\zeta) \rangle\right)^2\right]^{1/2}. \quad (1)$$

With $W_b(\zeta) = N_b^{-1} \sum_{k=1}^{Nb} W_{b,k}(\zeta)$ corresponding to the average bootstrapped PMFs at the coordinate ζ. The reader is directed to the original reference of the bootstrap implementation for further details [56]. However, we should point out that deficient sampling in the umbrella sampling windows may substantially underestimate the statistical error in the bootstrap procedure and, therefore, the reported errors should be looked as a lower bound estimate of the statistical error.

3. Results and discussion

3.1. **CX-1** *diffusion across the DOPC membrane model*

As mentioned earlier, the calixarene derivative **CX-1** was initially placed in the water slab (system **B**) or in the membrane core (system **C**). The distance between the calix[4]arene to the membrane along the z direction throughout the simulation time was monitored for all replicates and is plotted in Fig. 1. The membrane interface is defined as the average z coordinate of the phosphorus atoms in the closest layer, whereas the position of **CX-1** is determined through two z coordinates: the distance of the center of mass defined by the four $-NH_3^+$ binding groups (N^{COM}) and the center of mass determined by the $-CH_3$ groups of the four aliphatic tails (C^{COM}), highlighted in Fig. 2, relatively to the interface. Thus, positive values ($z > 0$) indicate that **CX-1** is in the water phase while negative values ($z < 0$) indicate that **CX-1** is inside the membrane.

The three replicates of system **B** behave slightly different showing that different scenarios were sampled throughout the simulation time.

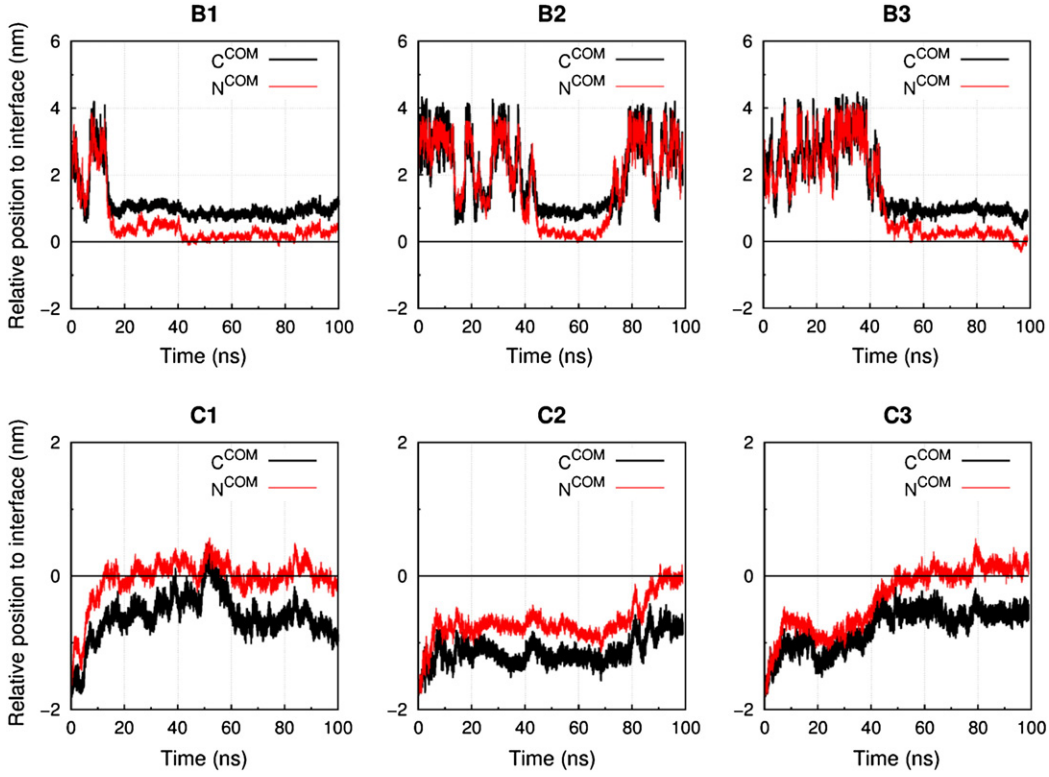

Fig. 1. Position of **CX-1** relative to the closest membrane interface ($z = 0$ nm) for three replicates of systems **B** and **C**. **CX-1** is represented by the center of mass defined by four $-NH_3^+$ groups (N^{COM}) and the center of mass defined by four $-CH_3$ groups of the aliphatic tails (C^{COM}).

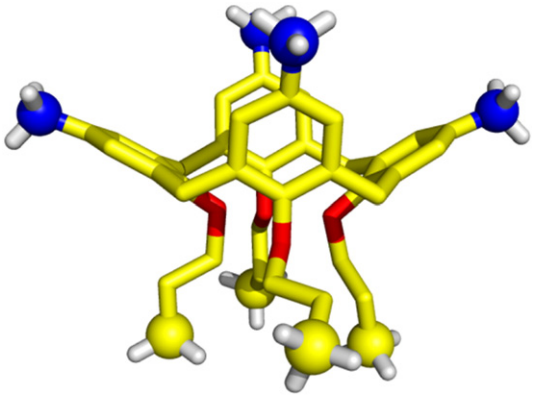

Fig. 2. DFT (B3LYP) gas-phase structure of **CX-1** with carbon atoms represented in yellow, oxygen in red, and nitrogen in blue. Hydrogen atoms, apart those from $-NH_3^+$ and $-CH_3$ were omitted for clarity. The nitrogen and the carbon atoms contributing for N^{COM} and C^{COM} are drawn as spheres.

In both **B1** and **B3** simulations, **CX-1** reaches the interface, remaining there with N^{COM} often crossing the interface ($z < 0$) while simulation **B2** reveals an interesting sequence of events as it shows the reversible binding of **CX-1** to the membrane. This reversibility is important in the development of anion transporters, such as **CX-1**, considering that, if the molecule irreversibly binds to the lipid headgroups, it would not be able to fulfill its function as a mobile carrier. In spite of the small differences, all replicates show very clearly that the interaction of **CX-1** with the membrane occurs *via* the $-NH_3^+$ groups which are able to establish electrostatic interactions and multiple N–H···O═P hydrogen bonds with the DOPC phosphate groups while the aliphatic tails point towards the water phase. This does not correspond to the expected orientation, as reported before for related cationic calix[4]arenes [20], where the lower rim aliphatic tails are immersed in the lipid core while the upper rim polar groups are near the lipid heads. However, starting from setup **B**, **CX-1** would have to rotate and insert its hydrophobic tails in the membrane core. It has also been reported that there is an energetic barrier required for charged species to cross a phospholipid bilayer interface from the water phase [57,58], however, such barrier was not found in our PMF curves (*vide infra*).

Simulations of system **C** allow to evaluate how **CX-1** behaves inside the hydrophobic environment provided by the bilayer moiety, partially overcoming the fact that in replicates **B1**–**B3** no internalization was observed for each 100 ns replicate. A noteworthy feature present in all three MD replicates of **C** (see Fig. 1) is the ability of **CX-1**, in spite of its size, to diffuse within the highly packed media of the lipid tails and direct itself towards the membrane interface at different times (~18 ns, ~90 ns, and ~50 ns for **C1**, **C2**, and **C3**, respectively), but not being released to the water phase. **CX-1** is clearly oriented, with the $-NH_3^+$ groups pointing towards the membrane interface, while the $-CH_3$ groups of the aliphatic chains are immersed in the lipid chains below the phosphorus positions ($z < 0$). The dipole moment of **CX-1** tends to align in the z direction, with its z component oscillating around its maximum as shown in Fig. S2 (left plot) for replicate **C1**. The orientation of **CX-1** can also be described by the variation of the C^{COM}···N^{COM} tilt angle, which is defined by the angle of the C^{COM}···N^{COM} axis, relative to the bilayer normal (z). Thus, the evolution of the tilt angle throughout the simulation time for replicate **C1**, presented in Fig. S2 (right plot), indicates a preferential alignment of **CX-1** with the z direction. This is particular evident for the last 15 ns of MD simulation in which the tilt angle ranges between 150 and 180°. This orientation is in total agreement with the parallel orientation experimentally determined for amphiphilic calix[4]arene molecules inside stearic acid monolayers [19,20] which would correspond to tilt angles of ~180° or 0°, depending on the interface.

A curious sequence of events occurs in replicate **C1** around 50 ns simulation time, as shown in Fig. 3, which might indicate that **CX-1** could eventually be released from the DOPC membrane in agreement with the experimental results [16]. Indeed, **CX-1** is aligned inside the bilayer until *ca.* the first 29 ns of simulation time, then starting to rotate with one aliphatic tail approaching the water phase ($t \approx 48$ ns), and eventually, one terminal methyl group of an ether chain of **CX-1** becomes completely immersed in the water phase ($t \approx 49$ ns). The process continues and the maximum rotation occurs at *ca.* 50.7 ns when the highest value of the "C^{COM}–membrane" distance (0.48 nm) is achieved and the z component of **CX-1** dipole moment reaches zero, as the molecule N^{COM}–C^{COM} axis is perpendicular to the bilayer normal (Fig. S2, left). This corresponds to a C^{COM}···N^{COM} tilt angle of ~90° (Fig. S2, right). The scenario at 50.7 ns presented in Fig. 3 is relatively close to some

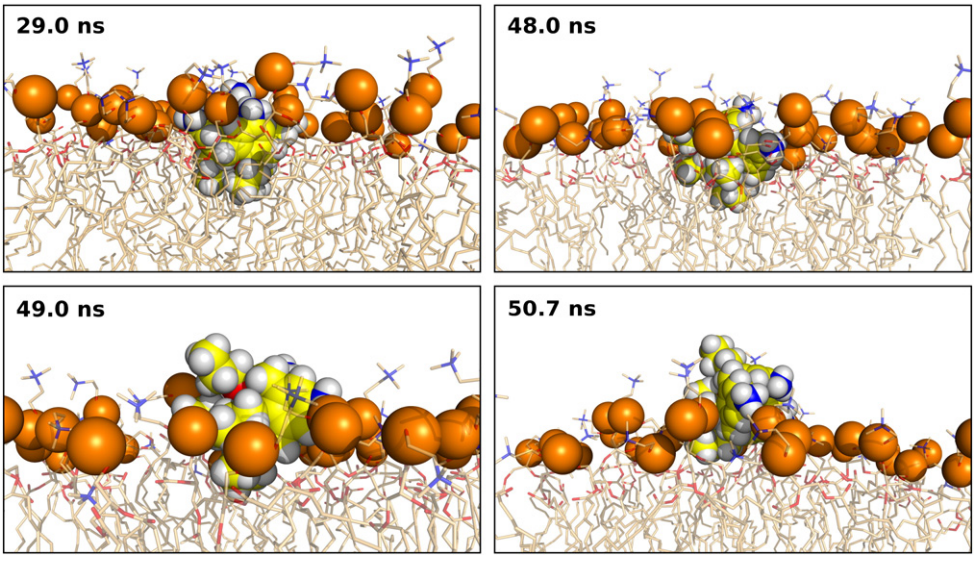

Fig. 3. Snapshots taken from the MD simulation of replicate **C1** illustrating the rotation processes of **CX-1**.

arrangements observed in MD replicates of system **B**, showing that conversion from scenario **C** to **B** could be possible, although not completely observed.

3.2. Effects of *CX-1* on the biophysical properties of the DOPC membrane

The area per lipid, A_L, is often used to check if a membrane simulation is properly equilibrated and most importantly, if the liquid-crystalline state is maintained. Previous simulation results showed that an NPγT ensemble must be used with the GAFF in order to prevent a phase transition to a more ordered gel-like state [39] as it was observed in an NPT simulation without surface tension [38]. In our simulations, A_L was calculated, as usually, from the lateral dimensions (x, y) of the simulation box divided by the number of lipids in each leaflet and the values obtained for all simulations are summarized in Table 1.

Our control simulation **A**, as expected, yielded an identical A_L value to the previous one reported in Ref. [39] which in turn was in perfect agreement with the experimental value (0.72 nm^2) [59,60]. This shows that a larger water cap has marginal or no impact on the calculated A_L value. Furthermore, we were interested in the effect that **CX-1** might have in the A_L values since, for instance, a π-A isotherm expansion of 0.08 nm^2 was observed for the incorporation of ~40% (of 0.13 equiv) of a similar anilinium calix[4]arene into a stearic acid monolayer [20]. The values collected for the replicates of system **B** indicate a slight increase in A_L in the order of 1%, which can be considered negligible since it is within the standard deviation. In this context, an increase of ~5% on average observed in the value of A_L for system **C** is noticeable. In fact, given the relative size of **CX-1**, it is not difficult to rationalize that this molecule embedded in the membrane core causes a small expansion on the x, y dimensions of the simulation box, yielding a higher A_L value in agreement with the experimental results [20]. The variation of A_L throughout the simulation time for each replicate is presented in Fig. S3.

Another structural parameter used to characterize a membrane is the bilayer thickness, D_{HH}, which is commonly calculated as the distance between the two peaks in the electron density profiles (see Fig. S4 for the individual plots). The D_{HH} values given in Table 1 can be directly compared with the experimental values 3.71 nm [59] and 3.53 nm [61]. In the control simulation **A** a peak-to-peak distance of 3.51 nm was obtained, comparing fairly with the experimental value 3.53 nm and the previous simulated value in identical conditions, 3.61 nm [39]. Normally, an increase in the area per lipid is accompanied by a decrease of the membrane thickness [62] and *vice-versa* [3]. In our simulations of system **B**, even though the A_L remained practically constant when compared with system **A**, there is a slight increase of D_{HH} (except for replicate **B2**). The same increase in D_{HH} was observed for simulations **C1** and **C2** of system **C**.

If one wants to follow the variation of the membrane thickness with the simulation time and relate it with the relative distance of **CX-1** to the membrane interface, the use D_{HH} is not straightforward. Therefore, an alternative thickness measure was also used, D_{PP}, defined as follows

$$D_{PP}(t) = \left|\langle P_1^z(t)\rangle - \langle P_2^z(t)\rangle\right| \quad (2)$$

where $\langle P_1^z(t)\rangle$ and $\langle P_2^z(t)\rangle$ correspond to the individual z coordinates of the phosphorus atoms in the first and second individual layers respectively at a given simulation time t = t, averaged over the 36 atoms in each layer. This allows plotting the *instantaneous* D_{PP} values for each t of an MD simulation (Fig. S5, red line) and relate them with the N^{COM} and C^{COM} distances to the closest membrane interface as defined above. In replicates **B1** and **B2**, D_{PP} is relatively independent of the distance of **CX-1** to the interface. On the other hand, in replicate **B3**, when the calix[4]arene approaches the interface after the first 40 ns of MD simulation, the $<D_{PP}>$ values drop from a stable plateau. This plateau is recovered *c.a.* 15 ns later until the end of simulation (Fig. S5). The simulations with system **C** show a tendency for an increase in the D_{PP} values as **CX-1** approaches the interface, except for **C1** where D_{PP} remains relatively stable during the simulation time. Overall, small variations are observed in D_{PP}, but no drastic changes were observed upon DOPC membrane interaction with **CX-1**, except for the replicate **B3** where a sudden decrease of D_{PP} was observed with the interaction as mentioned above.

The hydration of the phospholipid heads was also evaluated through the calculation of the average number of water molecules at distances lower than a 0.35 nm radius from the individual choline and phosphate headgroups for the last 20 ns of unconstrained MD simulations. The values calculated for each replicate of systems **B** and **C,** also collected in Table 1, are very similar and close to an average of 14 water molecules, slightly larger than the experimental value (~12) [63] or the simulated one in an NPT ensemble (12.5) [38]. No particular changes were observed upon interaction with **CX-1** as evident when the estimated values for systems **B** and **C** are compared with the corresponding value for the overhydrated system **A**.

The deuterium lipid order parameters $|S_{CD}|$, given by

$$|S_{CD}| = \frac{1}{2}\left\langle\left(3\cos^2\theta_i - 1\right)\right\rangle \quad (3)$$

where θ_i is the angle between the bilayer normal and the C_i–H bond, were calculated using MOLDY tools [64]. The values correspond to the average calculated over the 80 ns collection time. The behavior of our control simulation **A** plotted in Fig. S6 is similar to the one previously reported [39] with a dip at the C11 carbon atom of the *sn-1* tail and at both C10 and C11 carbon atoms on the *sn-2* tail. Moreover, a larger order was observed for the C2 carbon atom of the *sn-1* tail, an experimental feature that only GAFF was able to reproduce in the original paper. The effect that **CX-1** produces in the order parameters is seen in the $|S_{CD}|$ values for systems **B** and **C** plotted together with those estimated for the control simulation **A** in Fig. 4. A striking difference between systems **B**-**C** and **A** is that the order of the C2 carbon atom of the *sn-1* tail is greatly reduced upon interaction with **CX-1**, meaning that the C-H axis is on average more perpendicularly aligned to the bilayer normal than on the control simulation. This effect was systematic as it was observed in all replicates of systems **B** and **C**. No other significant deviations were found for the remaining carbon atoms, showing that the interaction of **CX-1** with the DOPC membrane occurs near the headgroup region.

Overall, the unconstrained MD simulations show that **CX-1** is able to interact with the DOPC bilayer with only small structural changes on the bilayer structure. This is a very important feature for an anion

Table 1
Average area per lipid (A_L), bilayer thickness (D_{HH}), and phospholipid hydration for all individual replicates of systems **A**, **B**, and **C**. The errors correspond to the standard deviations.

System	A_L (nm^2)	D_{HH} (nm)	Hydration[a]
A	0.72 ± 0.02	3.51	13.6 ± 0.3
B1	0.73 ± 0.02	3.59	13.5 ± 0.3
B2	0.74 ± 0.02	3.51	13.7 ± 0.4
B3	0.73 ± 0.02	3.66	13.5 ± 0.3
C1	0.73 ± 0.01	3.71	13.6 ± 0.3
C2	0.80 ± 0.03	3.79	13.9 ± 0.3
C3	0.76 ± 0.02	3.52	13.7 ± 0.4
Experimental	0.721[b]	3.71[b], 3.53[c]	~12[d]
GAFF + SPC/E (NPγT)[e]	0.72	3.61	–
GAFF + TIP3P (NPT)[f]	0.65	3.84	12.5

[a] The number of hydration water molecules was calculated for the last 20 ns of MD simulation.
[b] Values from Ref. [59].
[c] Value from Ref. [61].
[d] Value from Ref. [63].
[e] Values from Ref. [39].
[f] Values from Ref. [38].

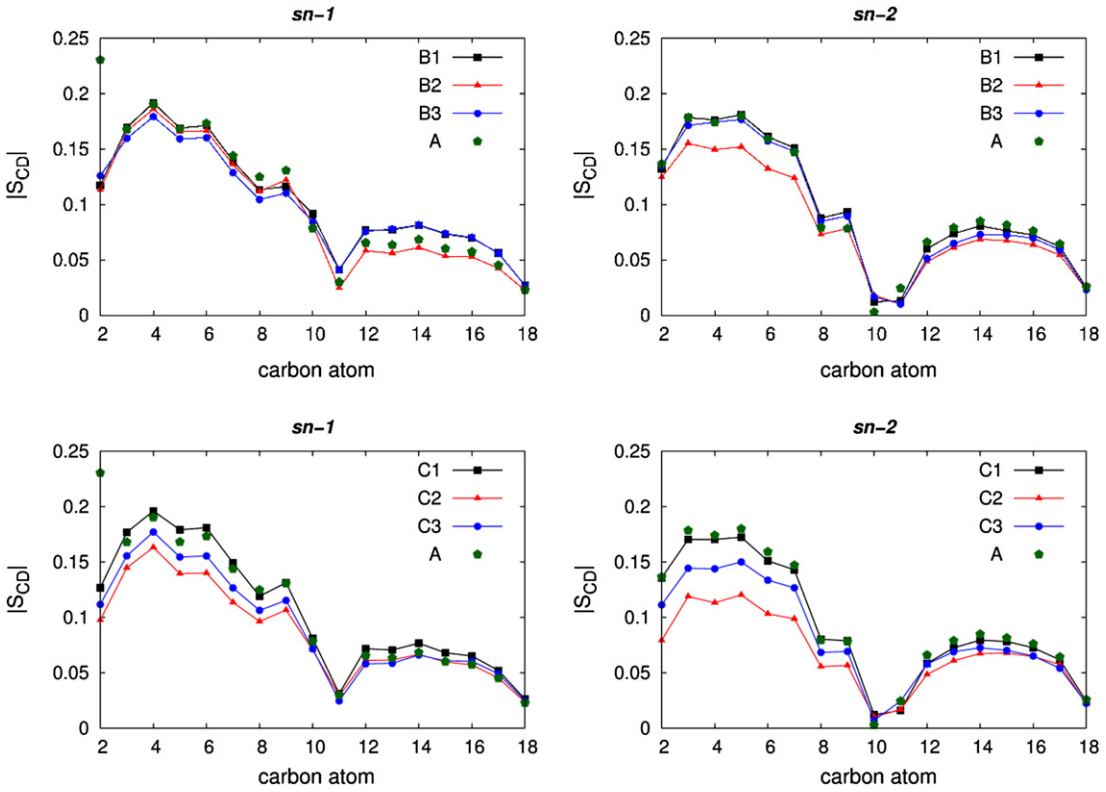

Fig. 4. Calculated deuterium lipid order parameters, $|S_{CD}|$, for the *sn-1* (left) and *sn-2* (right) chains of systems **B** (top) and **C** (bottom). Values obtained for system **A** are also plotted for comparison purposes.

transporter candidate, considering that this type of molecules should preserve the membrane integrity upon interaction, not inducing cell necrosis.

3.3. Pulling simulations: *CX-1* as a possible transmembrane chloride transporter?

As mentioned earlier, **CX-1** might constitute a potential transmembrane anion carrier since it possesses groups capable of anion binding and ether lipophilic chains able to internalize **CX-1** in a lipid bilayer. However, in the unconstrained MD simulations presented in Section 3.1, spontaneous chloride transport across the DOPC membrane promoted by **CX-1** was not observed. Since experimentally there is no doubt that **CX-1** is internalized in the cell [16], we tried to simulate this event on a DOPC bilayer by biasing our simulation with a harmonic potential which pulls **CX-1** with a constant velocity, *i.e.* a constant velocity steered molecular dynamics (SMD) simulation. Succinctly, in this type of simulation, the system is guided by an external harmonic potential in such a way that it is forced to move along a defined reaction coordinate. In our case, the obvious reaction coordinate is the *z* component defined by the distance from the COM of ***CX-1***, excluding all hydrogen, to the center of the bilayer. Three replicates were carried out as described above in Section 2.4. A similar strategy was used by our group on the investigation of the assisted transfer of KCl and dopamine through a water-chloroform interface [22] and in this earlier study, pull rates of 0.0025 nm ps^{-1} and 0.001 nm ps^{-1} were found appropriate. A 0.001 nm ps^{-1} pull rate was also used on SMD simulations of the insertion of a poly(alkylthiophene) conductive polymer into DMPC bilayers [65]. Since we intend, at least qualitatively, to mimic the observed internalization process of **CX-1**, we tested several pulling velocities ranging from 0.01 nm ps^{-1} to 0.001 nm ps^{-1}. These velocities correspond to diffusion coefficients in the *z* direction, D_z, ranging from 5×10^{-11} m^2/s to 5×10^{-13} m^2/s, which can be considered physically acceptable when compared with the experimental diffusion coefficient for pyrene in dipalmitoyllecithin membranes of $D = 1.4 \times 10^{-11}$ m^2/s (the value drops to 0.64×10^{-11} m^2/s if cholesterol is present) [66], while the simulated values for arabinoadenosine or 4-hydroxy-2-nonenal in a POPC membrane are $D = 5 \times 10^{-11}$ m^2/s [67] and $D = 2.3 \times 10^{-11}$ m^2/s [68], respectively. On the other hand, a value of $D = 2.7 \times 10^{-12}$ m^2/s was obtained for a Texas Red derivative in a DPPC membrane [69]. Nonetheless, despite using these slow pulling rates, these types of simulations are typically out of equilibrium and therefore, their interpretation should be taken with care.

In Table 2, a summary of the observed events during the pulling simulations is reported. If a pulling velocity of 0.01 nm ps^{-1} is used, no chloride transport is observed in all three replicates. The phospholipid bilayer suffers some structural deformation as **CX-1** is pulled inside (see Fig. S7) with some phosphate heads following the calix[4]arene and creating a small water cone inside the membrane. However, as soon as **CX-1** crosses the second interface, the bilayer relaxes, and its structural integrity is completely restored.

When the pulling velocity is reduced to values ranging from 0.0075 nm ps^{-1} to 0.001 nm ps^{-1}, very similar chloride transport events, assisted by **CX-1**, are observed in some replicates. Given their

Table 2
Summary of the observed events during the pulling simulations: "yes" and "no" mean that assisted transport of one chloride across the DOPC membrane was observed or not, respectively.

Pulling velocity nm ps^{-1}	Replicate 1	Replicate 2	Replicate 3
0.01	No	No	No
0.0075	Yes	No	Yes
0.005	Yes	No	Yes
0.001	Yes	No	Yes*

* Two chloride anions were transported.

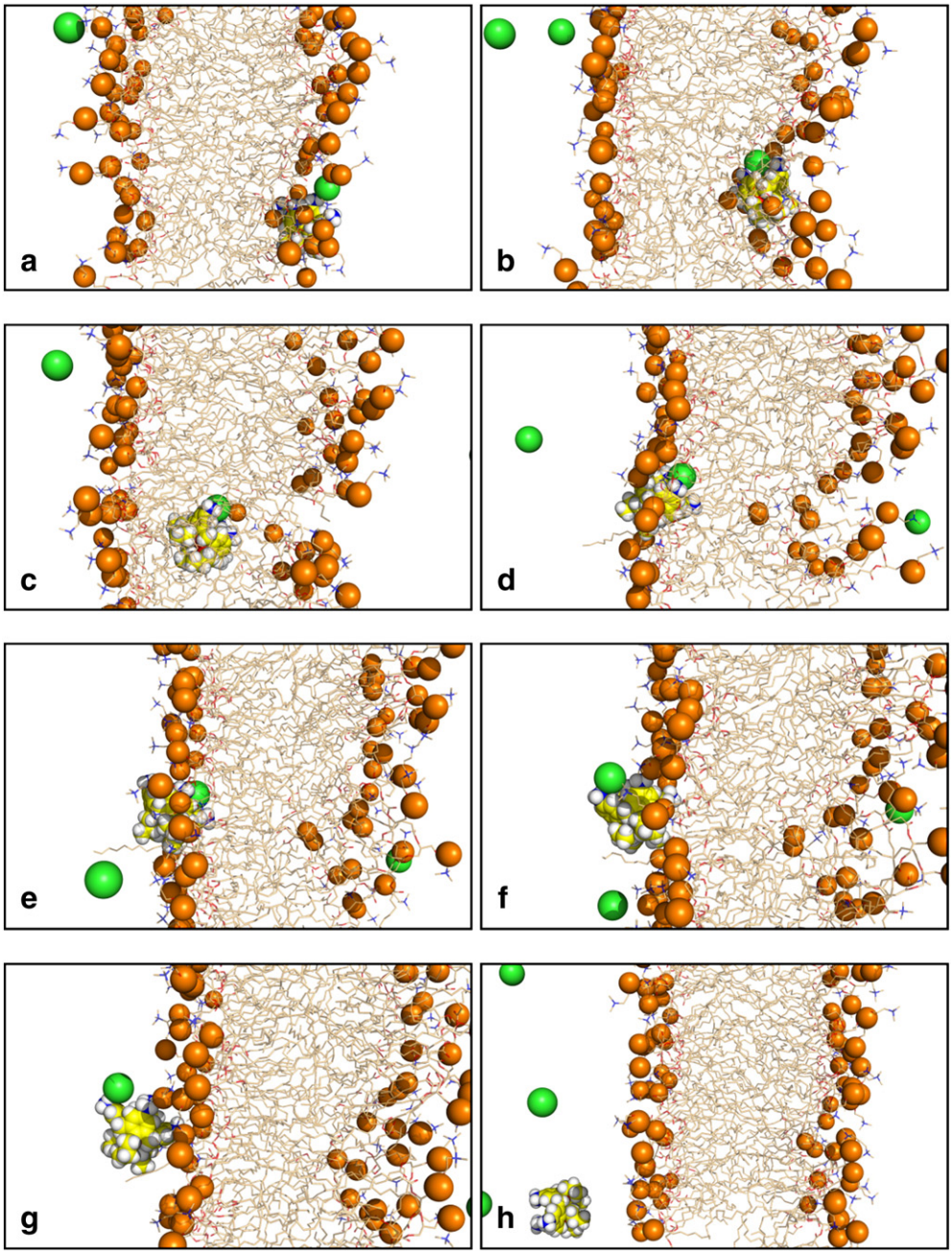

Fig. 5. Sequence of events, from a to h, illustrating chloride transmembrane transport assisted by **CX-1** in replicate 1. The system is being pulled from right to left at 0.001 nm ps^{-1}.

similarity, only the ones occurring at a pulling rate of 0.001 nm ps^{-1} will be thoroughly described. In Fig. 5 the sequence of relevant events observed along the replicate 1 is shown. The initial configuration corresponds to an equilibrated snapshot of the previously discussed unbiased simulations, where **CX-1** is in the water phase. The **CX-1** COM starts to be pulled towards the water-lipid interface and, during this period, some chloride anions establish sporadic interactions with **CX-1** until this species reaches the interface (Fig. 5a). At this stage, **CX-1** appears to orient itself in a parallel alignment relative to the interface in order to facilitate the crossing. We will return to **CX-1** reorientation below. It is noteworthy that a chloride approaches the **CX-1** $-NH_3^+$ groups, and subsequently crosses the phospholipid heads associated with **CX-1** (Fig. 5b). This event is accompanied by a deformation of the water-lipid interface in that specific region given that some phosphate heads also establish electrostatic interactions and hydrogen bonds with the positively charged $-NH_3^+$ binding groups and are also pulled inside along with the chloride anion (Fig. 5c). A small water cone that penetrates the region of the lipid tails is created concomitantly with the movement of **CX-1** across the water lipid interface, but, as the calix[4] arene starts to reach the other interface, the few bound phosphates start to unbound, returning to their respective leaflet (no phospholipid *flip-flop* was observed) with the disappearance of the water cone (Fig. 5d and e). At the second interface, **CX-1** is again aligned parallel to the interface with the chloride anion still bound, and, as the pulling proceeds, **CX-1** rotates and releases the chloride to the water bulk (Fig. 5f and g). The bilayer structure is preserved at the end of the simulation (Fig. 5h). It must be emphasized that, besides the *bias* introduced in the simulation by the pulling force, no constrain was introduced in the simulation to induce the assisted chloride transport through the membrane.

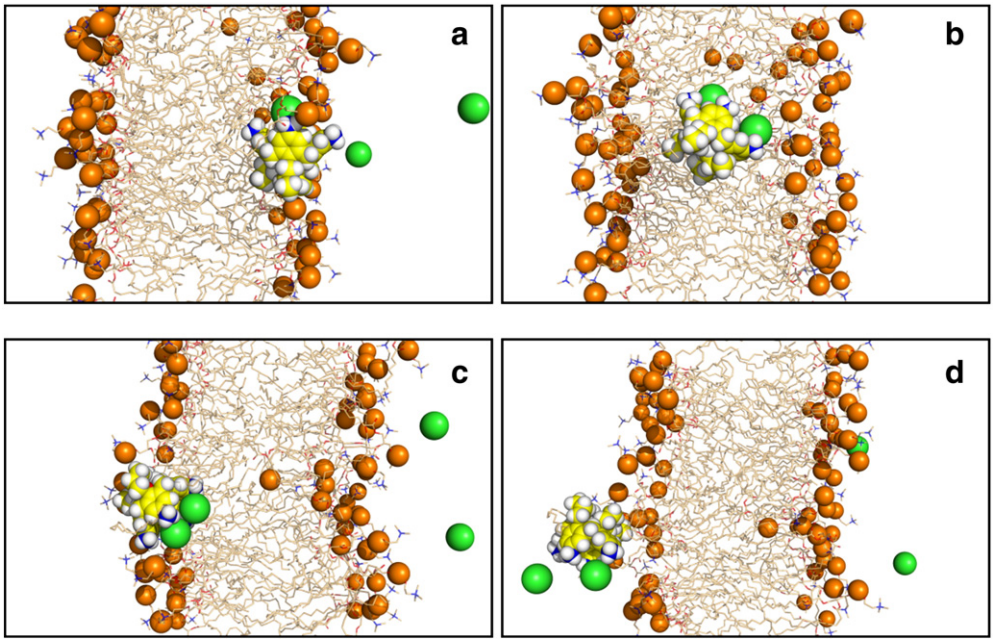

Fig. 6. Sequence of events from a to d illustrating transmembrane transport of two chloride anions assisted by **CX-1** in replicate 3. The system is being pulled from right to left at 0.001 nm ps^{-1}.

Replicate 3 is also remarkable since, instead of one single chloride being transported, the assisted passage of two anions is observed. Initially, the system behaves like replicate 1 with one chloride anion captured near the water-lipid interface (Fig. 6a) and goes across the interface bound to **CX-1**. While in the lipid phase, another chloride anion approaches, and taking advantage of the created water cone, also establishes an interaction with **CX-1**. Afterwards, the calix[4]arene moves towards the other interface keeping both chlorides attached (Fig. 6b), reaching it and eventually releasing both anions (Fig. 6c and d). Again, at the end of the simulation, the bilayer system conserves its structural integrity, thus showing that the transmembrane transport does not disrupt the membrane.

The force curves for the pulling of **CX-1** across the membrane with a constant velocity of 0.001 nm ps^{-1} are shown in Fig. 7 (left plot) for the three replicates. The maximum force recorded in these simulations was 580 kJ mol^{-1} nm^{-1} at $z = 0.8$, 1.0, and 0.6 nm for replicates 1, 2, and 3 respectively, *i.e.* close to the membrane center. Moreover, the relatively symmetrical shape of the curves is consistent with the fact that **CX-1** spontaneously moves to the water lipid interface in the unconstrained MD simulations. This force maximum is relatively high when compared with the force peak for poly(3-hexylthiophene) insertion in a DMPC bilayer (~335 kJ mol^{-1} nm^{-1}) [65], but compatible with the fact that a high amount of force is necessary to bring a charged species into the membrane core.

Another important issue is the required calix[4]arene reorientation inside the membrane, in order to act as a chloride transmembrane transporter. In Fig. 7 (right plot) is shown the variation of the $C^{COM}...N^{COM}$ tilt angle of **CX-1** throughout the pulling simulation time for all replicates. A tilt angle of 90° is indicative that **CX-1** is perpendicular to the bilayer normal whereas 0° and 180° represent parallel alignments, but in opposite directions. Analyzing the results from positive to negative *z* membrane depth values, outside the membrane ($z > 1.6$ nm) the vector defined by $C^{COM}...N^{COM}$ relative to *z* is able to oscillate with variations among replicates due to the stochastic motion/rotation of **CX-1** in water. However, as **CX-1** approaches the interface, the values start to converge to a maximum (~180°) meaning that, at the interface, **CX-1** is almost aligned with the bilayer normal. As the pulling continues, the tilt angle starts to approach 90°, as **CX-1** reaches the membrane core and gets increasingly more perpendicular to the bilayer normal. This alignment is reached at different *z* membrane depths for three replicates, but for all of them, as

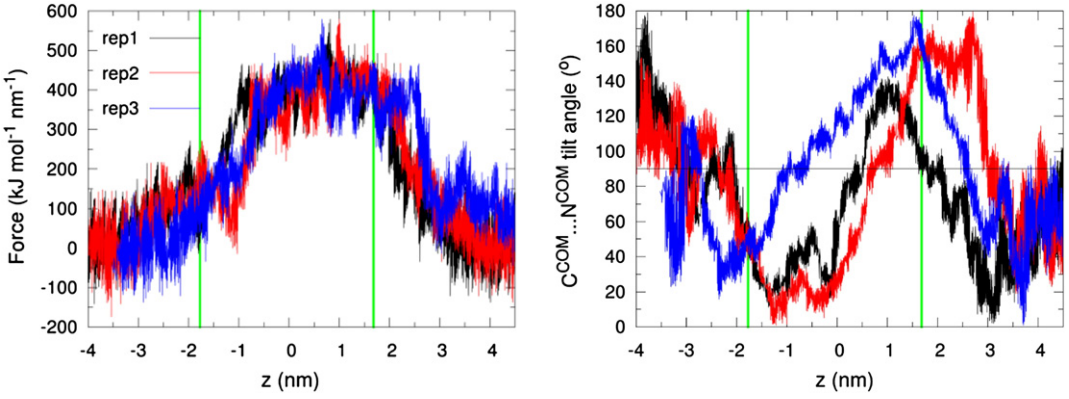

Fig. 7. Force profile for the **CX-1** membrane-crossing pathway with a pull rate of 0.001 nm ps^{-1} (left) together with the variation of the $C^{COM}...N^{COM}$ tilt angle throughout the pulling simulation time (right). $z = 0$ nm refers to the center of mass (COM) of the DOPC bilayer. The vertical green lines represent the average *z* position of the phosphorus atoms in the three replicates. The horizontal black line represents a tilt angle of 90°, meaning that **CX-1** is perpendicular to the bilayer normal.

the pulling continues, **CX-1** rotates and the angles become increasingly smaller than 90° and start to converge to a minimum (0°). At this point, the calix[4]arene is near the other interface, again, parallel to the bilayer normal. In the end, and despite the intrinsic non-equilibrium nature of these simulations, this rotation shows that the pulling rate was sufficiently low to allow, at least, a partial system adjustment.

The free energy associated with the insertion of **CX-1** into the DOPC bilayer is also of interest. Usually, the estimative of this energy barrier uses simulations performed along a single and intuitive reaction coordinate such as the distance between the solute and the bilayer center along the bilayer normal as in our pulling simulations. The corresponding Potential of Mean Force (PMF) curve can be extracted from SMD pulling simulations, applying the Jarzynski relationship [70], but several replicates are necessary in this case. Alternatively, this energy profile is commonly estimated *via* umbrella sampling simulations combined with the weighted histogram analysis method (WHAM). This methodology was followed in the current work, in spite of the fact that one degree of freedom can potentially be insufficient to describe the partitioning of a molecule through a membrane [71], due to the possible presence of hidden sampling barriers involving the slow reorganization of the lipid-water interface in response to that insertion, leading to convergence times exceeding 400 μs [72]. In our specific case, the reorganization of the ionic interactions between the positively charged (+4) **CX-1** and the negatively charged phosphate headgroups is expected to be very slow. Indeed, the fact that the phosphate heads follow **CX-1** inside the membrane in the pulling simulations is highly indicative of this situation. Moreover, these electrostatic interactions also contribute to the hindering of the rotation of **CX-1** in each simulation window (see below) and therefore contribute to sampling deficiencies in the PMF construction. The generation of fully converged sampling windows might require enormous simulations times in the μs time-scales, as mentioned earlier, [72,73] which are beyond our computational power. Therefore, although shorter simulations with only one degree of freedom do not possess enough accuracy to match the experimental data, they can still be very useful in the qualitative analysis of the diffusion phenomena through a phospholipid bilayer.

In this discussion, the PMF was obtained bringing **CX-1** from the membrane core to the water phase in the construction of the individual simulation windows and is depicted in Fig. 8, while the representative snapshots are given in Fig. S8. This approach minimizes the phosphate head pulling as described in Section 2.6. The PMF constructed using the opposite direction and its respective discussion are presented in Supplementary Material. The value $z = 0$ nm (a in Fig. 8) corresponds to **CX-1** positioned in the membrane core, similarly to the beginning of simulations **C**. As the z values increase, the energy starts to drop with a relatively high slope, being consistent with the fact that **CX-1** spontaneously migrates to the water lipid interface in the unconstrained simulations **C**. Eventually, the PMF reaches a minimum at $z = 1.42$ nm (b) with a -58 kJ mol^{-1} depth. In this situation, **CX-1** is near the water-lipid interface with the $-NH_3^+$ groups interacting with the phospholipid headgroups while the tails are still immersed in the lipid. This arrangement was preferred in the unconstrained simulations of system **C**, therefore consistent with a presence of an energy well and in agreement with the alignment observed experimentally for calixarenes in monolayers [19–21]. From this point onwards, as z increases, the PMF energy also increases until it reaches a plateau when **CX-1** is fully immersed in the water phase.

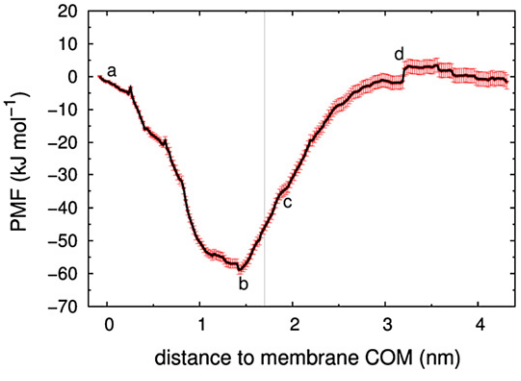

Fig. 8. PMF as a function of the **CX-1** distance to the membrane COM ($z = 0$ nm). The water-lipid interface, defined as the average position of phosphorus atoms is shown as a gray line. Error bars in red correspond to the statistical errors calculated using bootstrap analysis [56] and should be considered as lower estimates of the statistical uncertainty.

The **CX-1** distance to the membrane, by itself, is relatively easy to sample on each umbrella simulation window. However, proper conformational sampling requires, not only fulfilling the distance requirements, but also that the calixarene rotates on each window. To check this rotation, the $C^{COM}\cdots N^{COM}$ tilt angle was monitored throughout the collection period on each window (Fig. S9). Clearly, in the membrane core there is no rotational freedom as the calix[4]arene only experiments orientations with tilt values ~90°. As z increases, **CX-1** starts to be in parallel alignment with the bilayer normal (tilt angle ~0°) and again, a limited rotation is observed. With the approach of **CX-1** to the membrane interface, this behavior can be ascribed to the strong electrostatic interactions between the lipid headgroups and the highly charged **CX-1**, which inhibit the rotation, trapping the molecule in sampling barriers on each window [72]. Indeed, only at the water phase, corresponding to $z > 2.85$ nm, **CX-1** is able to explore several $C^{COM}\cdots N^{COM}$ tilt angles.

Overall, the energy profile estimated for **CX-1** with the calixarene starting on the membrane core indicates that there is a 58 kJ mol^{-1} barrier for this mobile carrier to cross the membrane center and was able to find the minimum that simulations **C** preferentially sampled. This barrier is large and inconsistent with the experimental time-scale reported for **CX-F** membrane uptake (the fluorescent derivative of **CX-1**) for which incubation times of only 10 min were needed [16]. For instance, a barrier of 75 kJ mol^{-1}, estimated for lipid *flip-flop* in a DPPC bilayer, leads to average lifetimes in the order of ~4 h [73]. Despite the fact that a DOPC bilayer is only a rough model of a cell membrane and other effects, *e.g.* ionic strength, pH, are not considered in our simulations, the discrepancy between the calculated value and the experimental observations is most certainly attributable to the fact that our PMF is not properly converged given the sampling limitations on each window. Nonetheless, the PMF provided useful insights into the process.

The PMF constructed in the opposite directions, *i.e.* from the water phase to the membrane center is discussed in detail in Supplementary Material. Nevertheless, it must be mentioned that in this case, another minima was found corresponding to the scenario to which simulations **B** converged. However, the pulling of several phosphate heads into the membrane core clearly makes this PMF less reliable than the one reported in Fig. 8. Moreover, the fact that both PMFs are not similar is indicative of a dependence on the starting configuration as well as that both PMFs were not fully converged.

4. Conclusions

MD simulations were used to gain insights, at the molecular level, of the interaction of a calix[4]arene derivative **CX-1** with a DOPC model bilayer and its potential ability to mediate the transmembrane chloride transport. The unconstrained MD simulations showed that, when **CX-1** is located in the water phase, it is able to migrate towards the interface and establish multiple N–H···O=P hydrogen bonds with the DOPC phosphate groups while the aliphatic tails point towards water. No full internalization was observed in the MD time-scale. When **CX-1** is put in the middle of the membrane, it also migrates towards the interface, remaining there with the $-NH_3^+$ binding groups near the lipid headgroups and the aliphatic ether tails immersed between the lipid

tails. Both starting scenarios do not disrupt the membrane structure being consistent with the experimentally observed cellular uptake.

We used constant velocity steered molecular dynamics (SMD) simulations to mimic the **CX-1** internalization in the membrane and, in this type of simulation, the chloride transport assisted by **CX-1** was observed for pulling rates of 0.0075, 0.005, and 0.001 nm ps^{-1}. In particular at the slower pulling rate, two chloride anions were transported by **CX-1** in one replicate simulation. This result shows that the $-NH_3^+$ can act as binding sites for anions while the aliphatic tails act as a lipophilic moiety facilitating membrane internalization, which is the rational normally followed in the design of synthetic receptors for transmembrane anion transport. We also estimated the barrier for the mobile carrier to cross the membrane to be *ca.* 58 kJ mol^{-1} by means of umbrella sampling simulations. However, this value should be carefully considered given the limitations of our PMF, eventually derived from an insufficient sampling.

The above results also show that MD simulations undertaken with GAFF are a powerful tool to study the interaction of synthetic transporters with biomembranes, as well as the corresponding ion transport mechanisms. It must be mentioned that, while the results of this paper were being analyzed, the dedicated AMBER lipid force field LIPID11 was released [74]. However, this new force field is largely based on the GAFF parameter set (excluding the charges), and therefore, the results obtained with LIPID11 would not be substantially different.

Acknowledgements

The authors acknowledge the financial support from QREN-FEDER through the Operational Program Competitiveness Factors – COMPETE and National Funds through FCT (Fundação para a Ciência e a Tecnologia) under project PTDC/QUI-QUI/101022/2008. P. J. C. thanks FCT for the postdoctoral grant SFRH/BPD/27082/2006 and project "New Strategies Applied to Neuropathological Disorders" (CENTRO-07-ST24-FEDER-002034), co-financed by QREN, Mais Centro - Programa Operacional Regional do Centro and União Europeia/Fundo Europeu de Desenvolvimento Regional. I. M. thanks FCT for the PhD grant SFRH/BD/87520/2012.

Appendix A. Supplementary data

Supplementary data to this article can be found online at http://dx.doi.org/10.1016/j.bbamem.2013.11.021.

References

[1] O.G. Mouritsen, Life—As a Matter of Fat: The Emerging Science of Lipidomics, Springer-Verlag, Berlin, 2004.
[2] B.W. Urban, Interactions of anesthetics with their targets: non-specific, specific or both? Pharmacol. Ther. 111 (2006) 729–770.
[3] R. Vacha, S.W.I. Siu, M. Petrov, R.A. Böckmann, J. Barucha-Kraszewska, P. Jurkiewicz, M. Hof, M.L. Berkowitz, P. Jungwirth, Effects of alkali cations and halide anions on the DOPC lipid membrane, J. Phys. Chem. A 113 (2009) 7235–7243.
[4] F.M. Ashcroft, Ion Channels and Disease, Academic Press, San Diego, 2000.
[5] C.J.E. Haynes, P.A. Gale, Transmembrane anion transport by synthetic systems, Chem. Commun. 47 (2011) 8203–8209.
[6] P.A. Gale, From anion receptors to transporters, Acc. Chem. Res. 44 (2011) 216–226.
[7] K.S.J. Iqbal, P.J. Cragg, Transmembrane ion transport by calixarenes and their derivatives, Dalton Trans. (2007) 26–32.
[8] A.K. Singh, R.K. Juneja, J.L. Atwood, R.J. Bridges, Para-sulfonato-calixarenes are potent blockers of colonic chloride channels, Biophys. J. 64 (1993) A17.
[9] A.K. Singh, C.J. Venglarik, R.J. Bridges, Development of chloride channel modulators, Kidney Int. 48 (1995) 985–993.
[10] E.M. Schwiebert, T. Flotte, G.R. Cutting, W.B. Guggino, Both CFTR and outwardly rectifying chloride channels contribute to cAMP-stimulated whole cell chloride currents, Am. J. Physiol. Cell Physiol. 266 (1994) C1464–C1477.
[11] S.M. Dudek, M.J. Friedlander, Intracellular blockade of inhibitory synaptic responses in visual cortical layer IV neurons, J. Neurophysiol. 75 (1996) 2167–2173.
[12] F. Perret, A.N. Lazar, A.W. Coleman, Biochemistry of the para-sulfonato calix[n] arenes, Chem. Commun. (2006) 2425–2438.
[13] I. Izzo, S. Licen, N. Maulucci, G. Autore, S. Marzocco, P. Tecilla, F. De Riccardis, Cationic calix[4]arenes as anion-selective ionophores, Chem. Commun. (2008) 2986–2988.
[14] V. Sidorov, F.W. Kotch, G. Abdrakhmanova, R. Mizani, J.C. Fettinger, J.T. Davis, Ion channel formation from a calix[4]arene amide that binds HCl, J. Am. Chem. Soc. 124 (2002) 2267–22278.
[15] O.A. Okunola, J.L. Seganish, K.J. Salimian, P.Y. Zavalij, J.T. Davis, Membrane-active calixarenes: toward 'gating' transmembrane anion transport, Tetrahedron 63 (2007) 10743–10750.
[16] R. Lalor, H. Baillie-Johnson, C. Redshaw, S.E. Matthews, A. Mueller, Cellular uptake of a fluorescent calix[4]arene derivative, J. Am. Chem. Soc. 130 (2008) 2892–2893.
[17] P. Shahgaldian, M. Cesario, P. Goreloff, A.W. Coleman, Para-acyl calix[4]arenes: amphiphilic self-assembly from the molecular to the mesoscopic level, Chem. Commun. (2002) 326–327.
[18] T. Schrader, Protein recognition: calixarene connection, Nat. Chem. 4 (2012) 519–520.
[19] R. Zadmard, M. Arendt, T. Schrader, Multipoint recognition of basic proteins at a membrane model, J. Am. Chem. Soc. 126 (2004) 7752–7753.
[20] R. Zadmard, T. Schrader, Nanomolar protein sensing with embedded receptor molecules, J. Am. Chem. Soc. 127 (2005) 904–915.
[21] S. Kolusheva, R. Zadmard, T. Schrader, R. Jelinek, Color fingerprinting of proteins by calixarenes embedded in lipid/polydiacetylene vesicles, J. Am. Chem. Soc. 128 (2006) 13592–13598.
[22] S.M. Santos, P.J. Costa, M.D. Lankshear, P.D. Beer, V. Félix, Molecular dynamics study of a heteroditopic-calix[4]diquinone-assisted transfer of kcl and dopamine through a water-chloroform liquid–liquid interface, J. Phys. Chem. B 114 (2010) 11173–11180.
[23] C.J.E. Haynes, S.J. Moore, J.R. Hiscock, I. Marques, P.J. Costa, V. Felix, P.A. Gale, Tunable transmembrane chloride transport by bis-indolylureas, Chem. Sci. 3 (2012) 1436–1444.
[24] S.J. Moore, C.J.E. Haynes, J. González, J.L. Sutton, S.J. Brooks, M.E. Light, J. Herniman, G.J. Langley, V. Soto-Cerrato, R. Pérez-Tomás, I. Marques, P.J. Costa, V. Félix, P.A. Gale, Chloride, carboxylate and carbonate transport by ortho-phenylenediamine based bisureas, Chem. Sci. 4 (2013) 103–117.
[25] L. Koubi, M. Tarek, S. Bandyopadhyay, M.L. Klein, D. Scharf, Membrane structural perturbations caused by anesthetics and nonimmobilizers: a molecular dynamics investigation, Biophys. J. 81 (2001) 3339–3345.
[26] L. Koubi, L. Saiz, M. Tarek, D. Scharf, M.L. Klein, Influence of anesthetic and nonimmobilizer molecules on the physical properties of a polyunsaturated lipid bilayer, J. Phys. Chem. B 107 (2003) 14500–14508.
[27] D. Bemporad, C. Luttmann, J.W. Essex, Behaviour of small solutes and large drugs in a lipid bilayer from computer simulations, Biochim. Biophys. Acta 1718 (2005) 1–21.
[28] F.E. Herrera, A. Bouchet, F. Lairion, E.A. Disalvo, S. Pantano, Molecular dynamics study of the interaction of arginine with phosphatidylcholine and phosphatidylethanolamine bilayers, J. Phys. Chem. B 116 (2012) 4476–4483.
[29] C.M. Dunkin, A. Pokorny, P.F. Almeida, H.-S. Lee, Molecular dynamics studies of transportan 10 (Tp10) interacting with a POPC lipid bilayer, J. Phys. Chem. B 115 (2011) 1188–1198.
[30] S.J. Irudayam, M.L. Berkowitz, Binding and reorientation of melittin in a POPC bilayer: computer simulations, Biochim. Biophys. Acta Biomembr. 1818 (2012) 2975–2981.
[31] L.M.S. Loura, A.M.T.M. Canto, J. Martins, Sensing hydration and behavior of pyrene in POPC and POPC/cholesterol bilayers: a molecular dynamics study, Biochim. Biophys. Acta Biomembr. 1828 (2013) 1094–1101.
[32] J. Wang, R.M. Wolf, J.W. Caldwell, P.A. Kollman, D.A. Case, Development and testing of a general amber force field, J. Comput. Chem. 25 (2004) 1157–1174.
[33] J.B. Klauda, R.M. Venable, J.A. Freites, J.W. O'Connor, D.J. Tobias, C. Mondragon-Ramirez, I. Vorobyov, A.D. MacKerell Jr., R.W. Pastor, Update of the CHARMM all-atom additive force field for lipids: validation on six lipid types, J. Phys. Chem. B 114 (2010) 7830–7843.
[34] D. Poger, W.F. van Gunsteren, A.E. Mark, A new force field for simulating phosphatidylcholine bilayers, J. Comput. Chem. 31 (2009) 1117–1125.
[35] D. Poger, A.E. Mark, On the validation of molecular dynamics simulations of saturated and cis-monounsaturated phosphatidylcholine lipid bilayers: a comparison with experiment, J. Chem. Theory Comput. 6 (2010) 325–336.
[36] B. Jojart, T.A. Martinek, Performance of the general amber force field in modeling aqueous POPC membrane bilayers, J. Comput. Chem. 28 (2007) 2051–2058.
[37] W.L. Jorgensen, J. Chandrasekhar, J.D. Madura, R.W. Impey, M.L. Klein, Comparison of simple potential functions for simulating liquid water, J. Chem. Phys. 79 (1983) 926–935.
[38] L. Rosso, I.R. Gould, Structure and dynamics of phospholipid bilayers using recently developed general all-atom force fields, J. Comput. Chem. 29 (2008) 24–37.
[39] S.W.I. Siu, R. Vacha, P. Jungwirth, R.A. Böckmann, Biomolecular simulations of membranes: physical properties from different force fields, J. Chem. Phys. 128 (2008) 125103.
[40] H.J.C. Berendsen, J.R. Grigera, T.P. Straatsma, The missing term in effective pair potentials, J. Phys. Chem. 91 (1987) 6269–6271.
[41] A.K. Malde, L. Zuo, M. Breeze, M. Stroet, D. Poger, P.C. Nair, C. Oostenbrink, A.E. Mark, An automated force field topology builder (ATB) and repository: version 1.0, J. Chem. Theory Comput. 7 (2011) 4026–4037.
[42] K. Vanommeslaeghe, E. Hatcher, C. Acharya, S. Kundu, S. Zhong, J. Shim, E. Darian, O. Guvench, P. Lopes, I. Vorobyov, A.D. Mackerell Jr., CHARMM general force field: a force field for drug-like molecules compatible with the CHARMM all-atom additive biological force fields, J. Comput. Chem. 31 (2010) 671–690.
[43] http://mackerell.umaryland.edu/kenno/cgenff/index.html(accessed in December 2012).

[44] J.M. Wang, W. Wang, P.A. Kollman, D.A. Case, Automatic atom type and bond type perception in molecular mechanical calculations, J. Mol. Graph. Model. 25 (2006) 247.
[45] L. Martinez, R. Andrade, E.G. Birgin, J.M. Martinez, PACKMOL: a package for building initial configurations for molecular dynamics simulations, J. Comput. Chem. 30 (2009) 2157–2164.
[46] M.J. Frisch, G.W. Trucks, H.B. Schlegel, G.E. Scuseria, M.A. Robb, J.R. Cheeseman, G. Scalmani, V. Barone, B. Mennucci, G.A. Petersson, H. Nakatsuji, M. Caricato, X. Li, H.P. Hratchian, A.F. Izmaylov, J. Bloino, G. Zheng, J.L. Sonnenberg, M. Hada, M. Ehara, K. Toyota, R. Fukuda, J. Hasegawa, M. Ishida, T. Nakajima, Y. Honda, O. Kitao, H. Nakai, T. Vreven, J.A. Montgomery Jr., J.E. Peralta, F. Ogliaro, M. Bearpark, J.J. Heyd, E. Brothers, K.N. Kudin, V.N. Staroverov, R. Kobayashi, J. Normand, K. Raghavachari, A. Rendell, J.C. Burant, S.S. Iyengar, J. Tomasi, M. Cossi, N. Rega, J.M. Millam, M. Klene, J.E. Knox, J.B. Cross, V. Bakken, C. Adamo, J. Jaramillo, R. Gomperts, R.E. Stratmann, O. Yazyev, A.J. Austin, R. Cammi, C. Pomelli, J.W. Ochterski, R.L. Martin, K. Morokuma, V.G. Zakrzewski, G.A. Voth, P. Salvador, J.J. Dannenberg, S. Dapprich, A.D. Daniels, Ö. Farkas, J.B. Foresman, J.V. Ortiz, J. Cioslowski, D.J. Fox, Gaussian 09, Revision A.1, Gaussian, Inc., Wallingford CT, 2009.
[47] A.W.S. Silva, E.D. Laue, W.F. Vranken, ACPYPE—AnteChamber PYthon Parser Interface, freely available at http://code.google.com/p/acpype/ (2010).
[48] B. Hess, C. Kutzner, D. van der Spoel, E. Lindahl, GROMACS 4: algorithms for highly efficient, load-balanced, and scalable molecular simulation, J. Chem. Theory Comput. 4 (2008) 435–447.
[49] H.J.C. Berendsen, J.P.M. Postma, W.F. van Gunsteren, A. Dinola, J.R. Haak, Molecular dynamics with coupling to an external bath, J. Chem. Phys. 81 (1984) 3684.
[50] T. Darden, D. York, L. Pedersen, Particle mesh Ewald: an N·log(N) method for Ewald sums in large systems, J. Chem. Phys. 98 (1993) 10089–10092.
[51] B. Hess, H. Bekker, H.J.C. Berendsen, J.G.E.M. Fraaije, LINCS: a linear constraint solver for molecular simulations, J. Comput. Chem. 18 (1997) 1463–1472.
[52] S. Miyamoto, P.A. Kollman, Settle: an analytical version of the SHAKE and RATTLE algorithm for rigid water models, J. Comput. Chem. 13 (1992) 952–962.
[53] B. Roux, The calculation of the potential of mean force using computer simulations, Comput. Phys. Commun. 91 (1995) 275–282.
[54] S. Kumar, J.M. Rosenberg, D. Bouzida, R.H. Swendsen, P.A. Kollman, THE weighted histogram analysis method for free-energy calculations on biomolecules. I. The method, J. Comput. Chem. 13 (1992) 1011–1021.
[55] M. Pourmousa, J. Wong-ekkabut, M. Patra, M. Karttunen, Molecular dynamic studies of transportan interacting with a DPPC lipid bilayer, J. Phys. Chem. B 117 (2013) 230–241.
[56] J.S. Hub, B.L. de Groot, D. van der Spoel, g_wham—a free weighted histogram analysis implementation including robust error and autocorrelation estimates, J. Chem. Theory Comput. 6 (2010) 3713–3720.
[57] L. Li, I. Vorobyov, A.D. MacKerell, T.W. Allen, Is arginine charged in a membrane? Biophys. J. 94 (2008) L11–L13.
[58] J. Yoo, Q. Cui, Does arginine remain protonated in the lipid membrane? Insights from microscopic pKa calculations, Biophys. J. 94 (2008) L61–L63.
[59] Y. Liu, J.F. Nagle, Diffuse scattering provides material parameters and electron density profiles of biomembranes, Phys. Rev. E 69 (2004) 040901.
[60] J. Pan, S. Tristram-Nagle, N. Kučerka, J.F. Nagle, Temperature dependence of structure, bending rigidity, and bilayer interactions of dioleoylphosphatidylcholine bilayers, Biophys. J. 94 (2008) 117–124.
[61] S. Tristam-Nagle, H. Petrache, J. Nagle, Structure and interactions of fully hydrated dioleoylphosphatidylcholine bilayers, Biophys. J. 75 (1998) 917–925.
[62] S. Witzke, L. Duelund, J. Kongsted, M. Petersen, O.G. Mouritsen, H. Khandelia, Inclusion of terpenoid plant extracts in lipid bilayers investigated by molecular dynamics simulations, J. Phys. Chem. B 114 (2010) 15825–15831.
[63] K. Hristova, S.H. White, Determination of the hydrocarbon core structure of fluid dioleoylphosphocholine (DOPC) bilayers by X-ray diffraction using specific bromination of the double-bonds: effect of hydration, Biophys. J. 74 (1998) 2419–2433.
[64] N. Whiteford, J. Taylor, MOLDY Tools, http://www.tchpc.tcd.ie/node/488 (2007).
[65] A.S. Widge, Y. Matsuoka, M. Kurnikova, Computational modeling of poly(alkylthiophene) conductive polymer insertion into phospholipid bilayers, Langmuir 23 (2007) 10672–10681.
[66] H.-J. Galla, E. Sackmann, Lateral diffusion in the hydrophobic region of membranes: use of pyrene excimers as optical probes, Biochim. Biophys. Acta Biomembr. 339 (1974) 103–115.
[67] C. Wei, A. Pohorille, Permeation of nucleosides through lipid bilayers, J. Phys. Chem. B 115 (2011) 3681–3688.
[68] M. Vazdar, P. Jurkiewicz, M. Hof, P. Jungwirth, L. Cwiklik, Behavior of 4-hydroxynonenal in phospholipid membranes, J. Phys. Chem. B 116 (2012) 6411–6415.
[69] M.J. Skaug, M.L. Longo, R. Faller, The impact of texas red on lipid bilayer properties, J. Phys. Chem. B 115 (2011) 8500–8505.
[70] C. Jarzynski, Equilibrium free-energy differences from nonequilibrium measurements: a master-equation approach, Phys. Rev. E 56 (1997) 5018–5035.
[71] Z. Ghaemi, M. Minozzi, P. Carloni, A. Laio, A novel approach to the investigation of passive molecular permeation through lipid bilayers from atomistic simulations, J. Phys. Chem. B 116 (2012) 8714–8721.
[72] C. Neale, W.F.D. Bennett, D.P. Tieleman, R. Pomès, Statistical convergence of equilibrium properties in simulations of molecular solutes embedded in lipid bilayers, J. Chem. Theory Comput. 7 (2011) 4175–4188.
[73] D.P. Tieleman, S.-J. Marrink, Lipids out of equilibrium: energetics of desorption and pore mediated flip-flop, J. Am. Chem. Soc. 128 (2006) 12462–12467.
[74] Å.A. Skjevik, B.D. Madej, R.C. Walker, K. Teigen, LIPID11: a modular framework for lipid simulations using amber, J. Phys. Chem. B 116 (2012) 11124–11136.